Available online at BCREC website: https://bcrec.id

Bulletin of Chemical Reaction Engineering & Catalysis, 14 (1) 2019, 142-152

Research Article

PEGylated MoS_2 Nanosheets: A Dual Functional Photocatalyst for Photodegradation of Organic Dyes and Photoreduction of Chromium from Aqueous Solution

Madima Ntakadzeni[1], William Wilson Anku[1]*, Neeraj Kumar[1], Penny Poomani Govender[1], Leelakrishna Reddy[2]

[1]Department of Applied Chemistry, University of Johannesburg, Doornfontein Campus 2028, Johannesburg, South Africa
[2]Department of Physics, University of Johannesburg, Doornfontein Campus 2028, Johannesburg, South Africa

Received: 22nd February 2018; Revised: 24th October 2018; Accepted: 30th October 2018; Available online: 25th January 2019; Published regularly: April 2019

Abstract

This article reports the synthesis of PEGylated microspheres of MoS_2 nanosheets through the hydrothermal method and its application in rhodamine B and methylene blue dyes photodegradation, and photoreduction of chromium(VI) to chromium(III) in water under illumination with visible light. The catalyst was characterized using X-ray Diffraction (XRD), Transmission Electron Microscopy (TEM), Field Emission Scanning Electron Microscopy (FESEM), Energy Dispersive X-ray Spectroscopy (EDS), Fourier Transform Infra Red (FTIR), Thermo-gravimetric Analysis (TGA), and UV-Vis spectroscopies. XRD result reveals the MoS_2 nanosheets to be present in the hexagonal phase of MoS_2. SEM, TEM, and HRTEM images show that the synthesised sample has spherical shapes made up of several thin sheets of MoS_2. The catalyst showed visible light responsivity with a calculated band gap of 1.92 eV. The MoS_2 nanosheets exhibited high degradation efficiency against both dyes. The RhB and MB dyes experienced degradation efficiencies of 97.30 % (RhB) and 98.05 % (MB) in 75 min 90 min, respectively. The MoS_2 photocatalyst is also observed to be effective in photocatalytic reduction of Cr(VI) and displayed 91.05% reduction of Cr(VI) to Cr(III) in 75 min. The results reveal that the synthesised MoS_2 nanosheet is a good photocatalytic material for degradation of dyes and reduction of Cr(VI) to Cr(III) in water.

Keywords: Photocatalyst; Photodegradation; Photoreduction; Dyes; Chromium, MoS_2

How to Cite: Ntakadzeni, M., Anku, W.W., Kumar, N., Govender, P.P., Reddy, L. (2019). PEGylated MoS_2 Nanosheets: A Dual Functional Photocatalyst for Photodegradation of Organic Dyes and Photoreduction of Chromium from Aqueous Solution. *Bulletin of Chemical Reaction Engineering & Catalysis*, 14 (1): 142-152 (doi:10.9767/bcrec.14.1.2258.142-152)

Permalink/DOI: https://doi.org/10.9767/bcrec.14.1.2258.142-152

1. Introduction

An increase in the world population together with the proliferation of factories and industrial development has led to increased energy crisis and environmental contamination [1]. Environmental contaminations issues are mostly associated with hazardous wastes, and toxic organic pollutants discharged into water bodies. Most of the coloured effluents emanating from industries, particularly the textile industries, contain

* Corresponding Author.
E-mail: williamanku85@gmail.com (W.W. Anku); krishr@uj.ac.za (L. Reddy)

toxic organic dyes and dyestuffs [2-4].

Heavy metals such as chromium (Cr) which is usually used in various applications including its use in alloys, steel manufacturing, chrome plating, leather tanning and wood processing [5,6] exists in the environment as a result of direct discharge from industries. It is regarded as a harmful entity owing to its highly toxic nature. Chromium exists in two different forms, i.e. Cr(VI) and Cr(III) with Cr(VI), being the most harmful form present in the aquatic environment. Dyes and Cr(VI) contaminated wastewater discharged from industries pollute water resources and pose life-threatening health effects to humans and wildlife [7]. As a result, issues relating to water pollution with heavy metals and organic dyes are receiving greater attention with a focus on the removal of dye molecules and Cr(VI) from wastewater before their final discharge into the environment.

Many efforts have been put into the removal of organic pollutants from wastewater due to the threat they pose to all forms of life. Recently, various techniques have been applied for the elimination of heavy metals and organic dyes from polluted water which includes chemical oxidation [8], extraction [9], adsorption [10], photocatalytic activity [11], and biochemical method [12]. Amongst them, photocatalytic degradation and photocatalytic reduction of organic pollutants and heavy metals using nanostructured photocatalyst semiconductor materials have been considered to be the most promising and sustainable strategies for water decontamination and environment remediation [13-15]due to their simplicity of design, low cost, flexibility and eco-friendliness [16,17]. Photocatalytic degradation of organic pollutants is a process that combines catalysis with solar radiation [18,19] to degrade the dyes into harmless compounds (CO_2 and H_2O) and also to reduce Cr(VI) into harmless Cr(III). In this regard, a photocatalytic semiconductor material absorbs light of energy more than or equal to its band-gap, resulting in electrons and holes generations followed by the formation of free radicals that are responsible for the oxidation of the contaminants.

Amongst the known photocatalyst, titanium dioxide (TiO_2) is the broadly used photocatalyst of choice due to the fact that it possesses certain peculiar features including strong oxidizing power, chemical stability, nontoxicity and low cost [20,21]. Irrespective of the various advantages, the use of TiO_2 and other photocatalysts in industrial scale photocatalysis is still restricted due to certain inherent shortfalls of these photocatalysts. These shortfalls include rapid recombination of excited charge carriers, poor chemical stability and wide band gap energies which only permits the catalysts to use ultraviolet (UV) light instead of the more abundant visible light. The UV light represents only about 4 % of the solar spectrum while the visible light accounts for about 45 % of the spectrum [22]. Therefore, it has become necessary to fabricate photocatalysts that are capable of utilizing visible light with efficient charge carriers separation abilities [23,24].

Molybdenum disulfide (MoS_2) is a low-cost, non-toxic and abundant semiconductor material with a small direct energy band gap (1.8 eV) in nanoscale and indirect energy band gap (1.2 eV) [25,26] in bulk form. It has been extensively used in electronics, energy conversion, and storage devices, but the potential of MoS_2 nanostructures in water purification and metal reduction has not been fully explored. In this study, we employed the one-step hydrothermal synthesis method to synthesize microspheres of MoS_2 nanosheets using polyethylene glycol (PEG) as a capping agent. The photocatalytic activity of the synthesized photocatalyst was explored for the photodegradation of Rhodamine (RhB), Methyl blue (MB) and photoreduction of Cr(VI) to Cr(III) in aqueous solution.

2. Materials and Method

2.1 Materials

Ammonium hexamolybdate tetrahydrate (AHM), polyethylene glycol (PEG, average M_n 400), thiourea, ethanol (99.8 %), methylene blue, rhodamine B, and potassium dichromate ($K_2Cr_2O_7$) were all obtained from Sigma-Aldrich and used without further purifications. Standard solution of the methylene blue and rhodamine B dyes were prepared through the dissolution of the appropriate masses of the dyes in deionized water (1000 mL). The desired dye concentrations (20 mg/L) were obtained through dilution of the prepared standard solutions. The Cr(VI) solution (10 ppm) was prepared by dissolving the calculated amount of $K_2Cr_2O_7$ in deionized water (1000 mL).

2.2 Synthesis of MoS_2 Nanosheets using PEG as a Capping Agent

The microsphere MoS_2 nanosheets were synthesised in a Teflon-lined autoclave via a hydrothermal route by using AHM and thiourea as the sources of molybdenum and sulphur, respectively. PEG-400 was used as a capping agent. The procedure of the preparation was as follows: A 1.200 g of AHM was dissolved

in 15 mL distilled water by a magnetic stirrer for 15 min. In another vial, 1.00 g of PEG-400 was also dissolved distilled water (15 mL). The PEG-400 solution was then introduced into the vial containing the AHM solution after which the mixture was stirred for 30 min. Thereafter, 2.400 g of thiourea was added the above mixture and the resultant mixture was stirred for another 20 min. The final solution was then transferred into 50 mL Teflon lined autoclave and reacted at 220 °C for 24 h. A black precipitate was obtained at the end of the reaction and was separated by centrifuging the suspension for 20 min (7830 rpm). The Black MoS_2 nanosheet was collected and washed several times with distilled water and ethanol. It was then dried in an oven overnight at 60 °C. A schematic diagram for the synthesis of the Pegylated microsphere MoS_2 nanosheets is presented in Scheme 1.

2.3 Materials Characterizations

The crystal structure of the product was investigated by X-ray diffraction (XRD) with Cu-Kα radiation (λ=0.15418 nm). The morphology and structure of the sample were characterized by transmission electron microscopy (TEM) and field emission scanning electron microscopy (FESEM) equipped with energy dispersive X-ray spectroscopy (EDS). Fourier transformed infrared (FTIR) spectrometer was used to detect the functional groups in the sample. Thermo-gravimetric analysis (TGA) was also performed to determine the thermal stability of PEGylated MoS_2 nanosheets. UV-Vis spectrometer was used for the determination of the energy band gap and also for the evaluation of photocatalytic activities.

2.4 Photocatalytic Experiment

2.4.1 Photodegradation of dye molecules

Photodegradation properties of the microsphere MoS_2 nanosheets were assessed by monitoring its ability to degrade RhB and MB dyes in aqueous solutions. In both experiments, 50 mg of the photocatalyst was dispersed in 100 mL (10 ppm) each of RhB and MB dye aqueous solutions. Prior to irradiation, the dye solutions with suspended photocatalysts in a round bottom flask were stirred in dark conditions to ensure that the surfaces of the catalysts were saturated with the dyes. The solutions were then placed in a photoreactor and were exposed to visible light under magnetic stirring conditions. The visible light was produced by attaching a UV filter to a solar simulator (250 W) which was the source of light for the experiment. At a regular time interval of 15 min, 4 mL of irradiated solutions of each dye was collected and centrifuged to remove the catalysts, and the supernatants were used for the evaluation of photodegradation. The su-

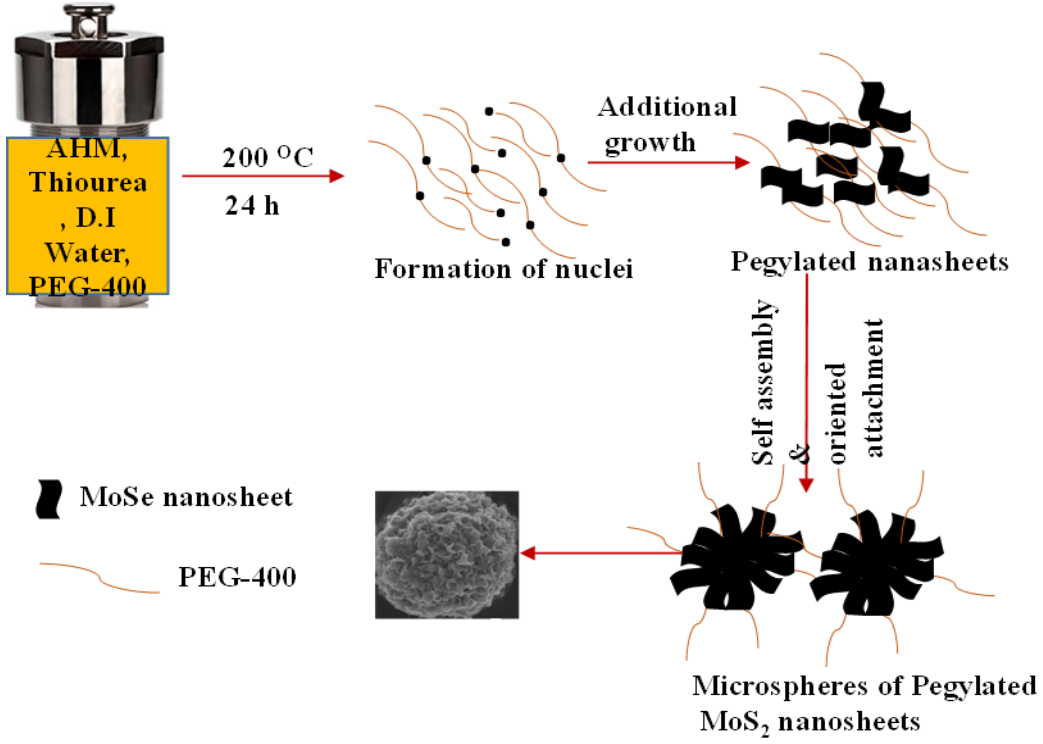

Scheme 1. A schematic diagram for the synthesis of the Pegylated microsphere MoS_2 nanosheets

pernatants were analysed using UV-Vis spectrophotometer to record the intensity of the absorption peaks of RhB (555 nm) and MB (665 nm).

2.4.2 Photoreduction of Chromium Cr(VI)

The photocatalytic performance of the synthesised catalyst was also evaluated through photocatalytic degradation of Cr(VI) under visible light irradiation. The photocatalyst (50 mg) was suspended in Cr(VI) solution (100 mL, 10 ppm) and the mixture was stirred for 20 min under a dark condition so as to attain adsorption-desorption equilibrium. Then, the suspension was illuminated with visible light for 75 minutes and at every 15 minutes intervals, 4 mL of the suspension was withdrawn and centrifuged to separate the photocatalyst and the Cr(VI). The process of photocatalytic reduction was monitored using UV-Vis spectrophotometer to record the intensity of the absorption peaks of Cr(VI) at 350 nm.

2.4.3 Catalyst recyclability study

The recyclability of the MoS_2 nanosheets for the degradation of RhB and MB dyes and reduction of Cr(VI) to Cr(III) was also performed by adhering to the procedure described in section 2.4.1 and 2.4.2, respectively. The reusability assessments were executed 5 successive times. At the end of each degradation cycle, the catalysts were separated from the solution by centrifugation. They were washed, dried at 60 ^{o}C for 12 h, and reused.

3. Results and Discussions

3.1 Characterizations

The morphologies of the synthesised microspheres of MoS_2 nanosheets were obtained via FESEM, TEM, and HRTEM. The FESEM image of the pure MoS_2 in Figure 1(a) clearly shows a cluster of MoS_2 thin sheets. That of the Pegylated MoS_2 (Figure 1(b)) is of microspherical shapes made up of several thin sheets of MoS_2. Thus, the PEG-400 played the role of a capping agent. TEM image from Figure 1(c) shows that the sample is made up of sheets of MoS_2. Figure1(d) which shows a high resolution-TEM image of the sample, reveals a layered structure of nanosheets. The distance between the adjacent layers was esti-

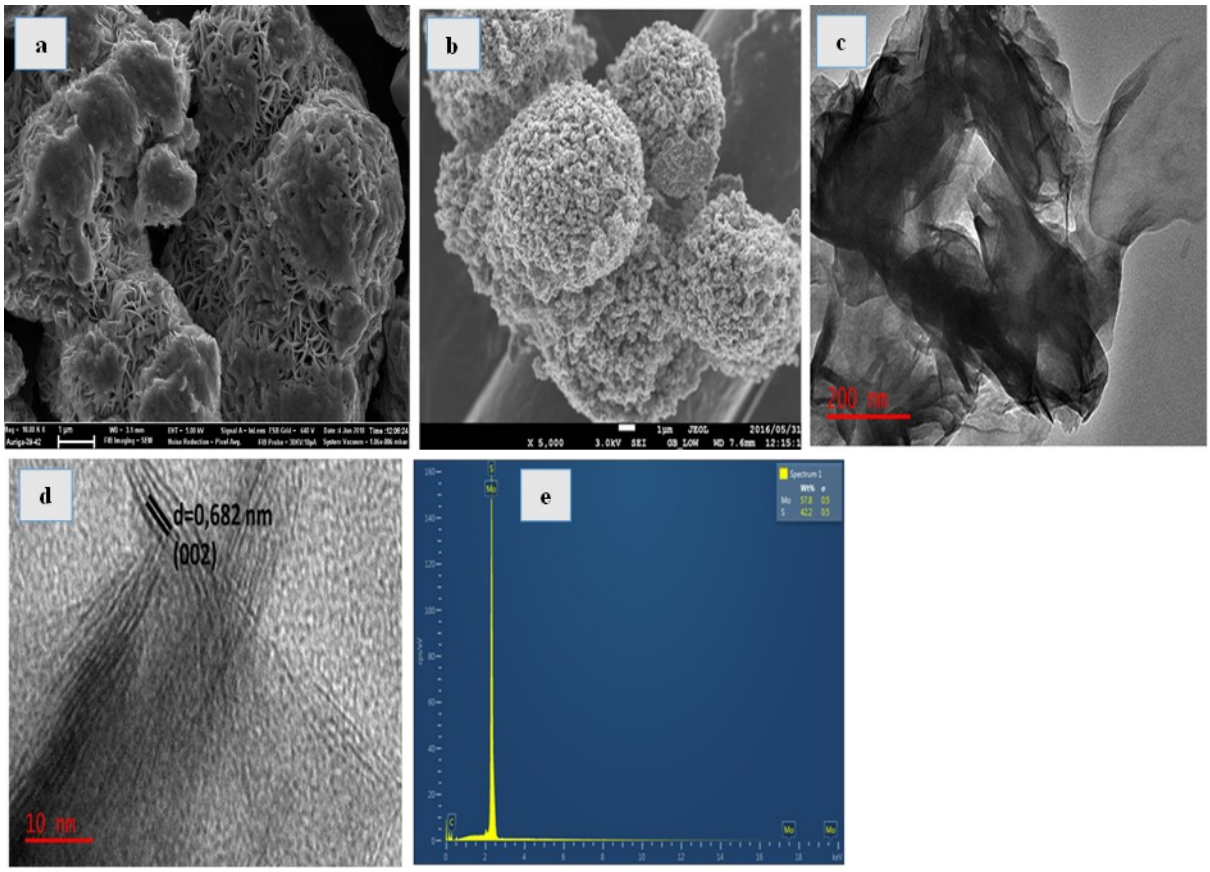

Figure 1. (a) FESEM image, (b) TEM image, (c) HRTEM image, and (d) EDX spectrum of the microspheres of MoS_2 nanosheets

mated to be 0.682 nm corresponding to (022) planes of hexagonal MoS_2 nanosheets. For the identification of elemental composition in the sample, SEM equipped with EDS was used. A typical EDS spectrum of MoS_2 shown in Figure 1(e) reveals the presence of Mo and S. The elemental C and O, come from the PEG-400 used as capping agents during the synthesis.

Figure 2 reveals the XRD pattern of the synthesized MoS_2 nanosheets. All the diffraction peaks are indexed as hexagonal MoS_2 (ICDD: 00-037-1492). The diffraction peak at 14.28° corresponds to (002) planes with a *d*-spacing of 0.620 nm which was calculated from Bragg's equation, whereas the d-spacing of pristine MoS_2, according to ICDD: 00-037-1492, is 0.612 nm indicating enlarged interlayer spacing in the nanosheets.

The peak at 33.96° correspond to (100) planes and indicates reduced spacing of 0.264 nm compared with 0.274 nm of pristine MoS_2. The two peaks at 40.27° and 60.28° correspond to (103) and (110) planes with *d*-spacing of 0.224 nm and 0.153 nm, respectively. The results prove that the PEGylated MoS_2 nanosheets were successfully prepared. The peaks were found to be broad which indicate smaller crystallite.

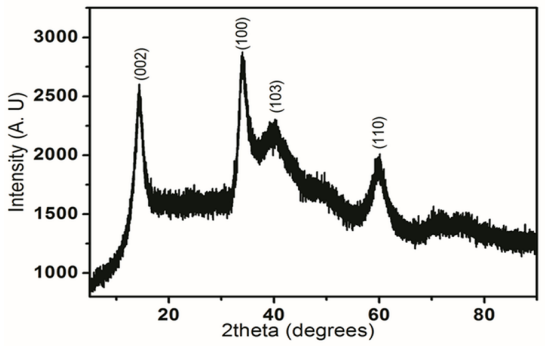

Figure 2. XRD pattern of the microspheres of MoS_2 nanosheets

Figure 3 illustrates the FTIR spectrum of the photocatalyst. Two vibrational modes at about 3435 and 1635 cm^{-1} are observed and assigned to the hydroxyl functionalities of adsorbed moisture from the atmosphere on the MoS_2 nanosheets. Figure 3(i), which is the inserted spectrum from 2800-3000 cm^{-1} range, shows the methyl symmetric and asymmetric stretches which are attributed to adsorbed PEG molecules on the MoS_2 nanosheets. The inserted spectrum of Figure 3(ii) which ranges from 400-500 cm^{-1}, exhibits a characteristic vibrational mode at 455 cm^{-1} and was assigned to the Mo-S linkage of the synthesised MoS_2 sample.

To assess the thermal stability of the prepared PEGylated MoS_2 nanosheets, TGA analysis of the sample was executed in the temperature range of 25 to 800 °C in air flow. The result is shown in Figure 4. The result shows four stages of weight lost. The first weight loss from 25 to 130 °C happens immediately after heating begins. This weight loss is assigned to the evaporation of absorbed water/moisture from the atmosphere.

The second stage of weight loss occurs from 245 to 340 °C and it is attributable to the decomposition of adsorbed polyethylene glycol molecules on the MoS_2 surfaces [32]. The third weight loss which occurred from 355 to 456 °C is assigned to the oxidation of MoS_2 to hexagonal-MoO_3 (h-MoO_3) and finally phase transformation to α-MoO_3. The last sharp stage of weight lost transpires possibly because of the decomposition of α-MoO_3.

UV-Vis spectrum (Figure 5 (a)) was obtained in order to probe the optical properties of the synthesized sample. The MoS_2 nanosheet demonstrates the ability to absorb light in the wavelength range of 200 to 800 nm. This indicates the ability of the catalyst to absorb light

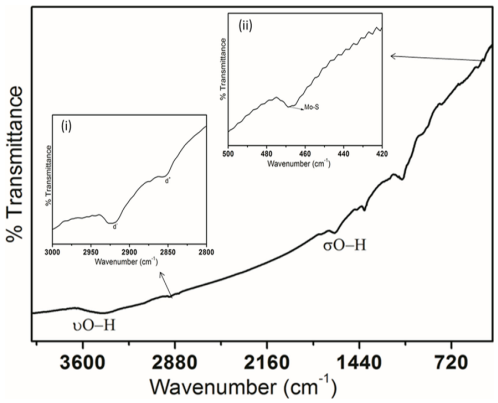

Figure 3. FTIR spectrum of the microspheres of MoS_2 nanosheets

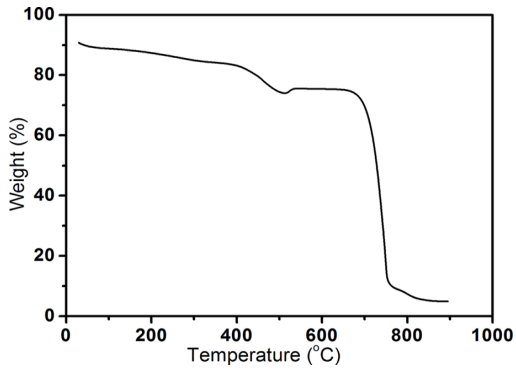

Figure 4. TGA curve of the microspheres of MoS_2 nanosheets

in both UV and visible light range of the electromagnetic spectrum.

The energy band of prepared MoS_2 nanosheets was calculated using equation (1):

$$\alpha h\nu = A\left(h\nu - E_g\right)^n \quad (1)$$

where α, υ, A, and E_g are the absorption coefficient, light frequency, proportionality constant and band gap energy, respectively. n describes the type of transition in the semiconductor.

MoS_2 exhibits a direct transition in nanoscale and indirect transition in bulk form, hence the value of n was taken as $^1/_2$ for the synthesised MoS_2 nanosheets. Figure 5(b) shows the energy band gap of the catalyst which was estimated from the plot of $(\alpha h\nu)^2$ versus $h\nu$ by extrapolating the straight line to X-axis intercept. The result indicates that the synthesised MoS_2 nanosheet has the energy band gap of 1.92 eV. This band gap value means that the MoS_2 nanosheet is visible light active and hence its ability to absorb light in the visible range (Figure 5(a)).

3.2. Photocatalytic Studies

3.2.1 Photocatalytic degradation of Rhodamine-B

Figure 6(a) illustrations the changes in the absorption spectrum of RhB dye with respect to irradiation time over the synthesised MoS_2 nanosheets. The typical absorption peak of RhB which occurs at 555 nm is noted to decreases progressively with an increase in irradiation time. This reduction in the peak intensity indicates the gradual degradation of the dye with increasing time. Figure 6(b) displays the photocatalytic degradation rate of RhB as a function of time with light and without irradiation with light. The concentration of RhB was observed to reduce progressively as the irradiation time increases.

The results also show that the rate of degradation of RhB by MoS_2 nanosheets in the presence of light is faster as compared to the degradation rate in the absence of light, which implies that light plays an important role in the

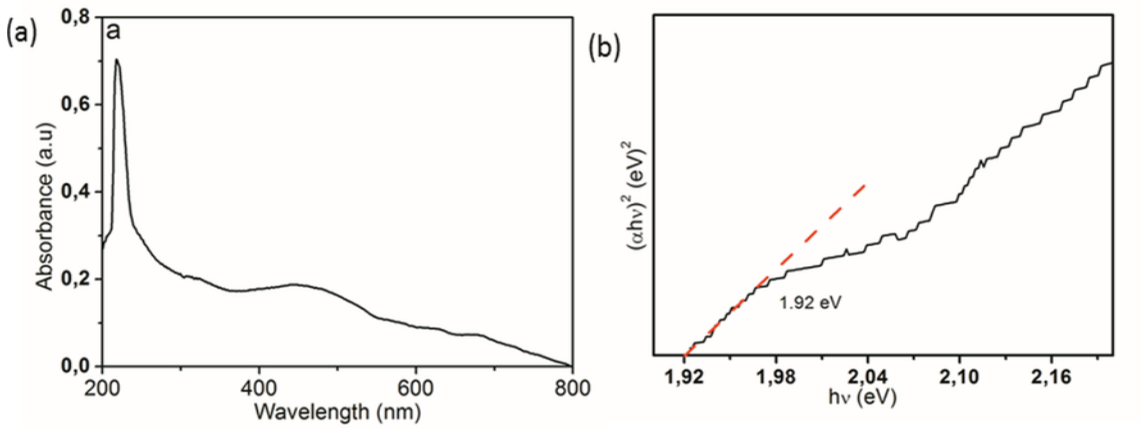

Figure 5. (a) UV–Vis and (b) Tauc plot estimated band-gap energy of the microspheres of MoS_2 nanosheets

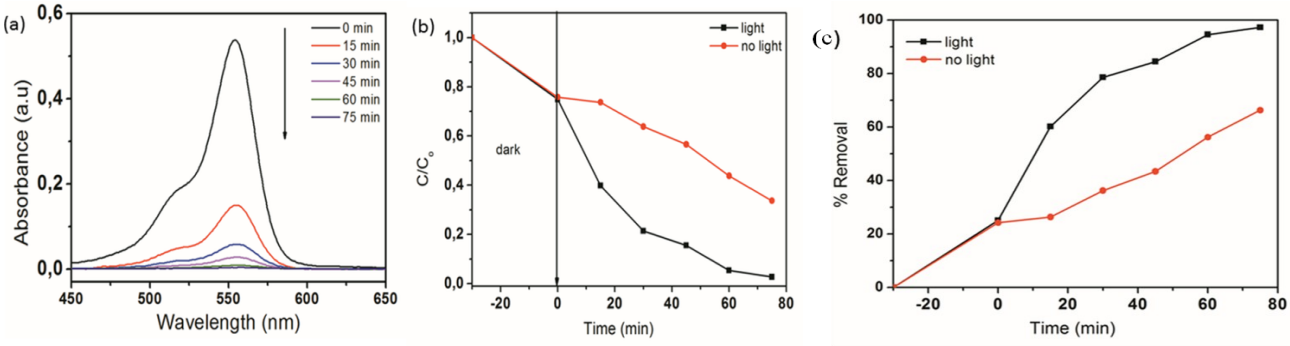

Figure 6. (a) UV–Vis spectroscopic changes of RhB aqueous solution in the presence MoS_2 nanosheets, (b) Photocatalytic degradation rate of RhB as a function of time and (c) Percent removal of RhB in the presence of MoS_2 nanosheets as a function of irradiation time

photodegradation of RhB. The reduction in the concentration of the dye in the dark can be attributed to adsorption of its molecules onto the surface of the catalyst which usually takes place prior to degradation.

The following equation was used to determine the % removal of RhB at a particular time *t*:

$$\%\,Removal = \left(1 - \frac{c}{c_o}\right) x100 \qquad (2)$$

It was observed that the prepared MoS_2 nanosheets showed greater efficiency in the degradation of RhB under light irradiation than in the absence of light, since the percentage removal in the presence of light was obtained to be 97.3 % and only 66.3 % was achieved in the absence of light as shown in Figure 6(c).

3.2.2 Photocatalytic degradation of Methyl Blue

The variation in the absorption spectrum of MB (10 ppm) dye with respect to irradiation time over the synthesised MoS_2 photocatalyst is shown in Figure 7(a). The characteristic absorption peak at 665 nm decreases with an increase in irradiation time. The photodegradation rate of MB is shown in Figure 7(b). The results show that the concentration of MB decreases as the irradiation time increases indicating a gradual degradation of the dye with increasing time. To determine removal efficiency of MB by MoS_2 nanosheets, the equation (2) was used. As evident from Figure 7(c), the prepared MoS_2 photocatalyst degrades 98.05 % of MB in 90 min. Thus the MoS_2 nanosheet exhibit high degradation efficiency against both RhB and MB dyes.

3.2.3 Chromium photoreduction studies

The photoreduction study was undertaken to evaluate the capability of MoS_2 nanosheets to photoreduce Cr(VI) to Cr(III). The UV-Vis absorption spectra of Cr(VI) reduction is presented in Figure 8. The figure shows a consistent decrease in the absorption spectrum of Cr(VI) with time in the presence of MoS_2 nanosheets which suggests that the Cr(VI) was gradually being converted to Cr(III) by the catalyst with increasing irradiation time. Figure 8(b) indicates the rate of Cr(VI) conversion as a function of time, and it was observed that the concentration of Cr(VI) decreases as the irradiation time increases. These observations mean the Cr(VI) become progressively converted to Cr(III) with increasing time. In order to investigate the role of kinetics on the photocatalytic reduction of Cr(VI), the plot of $-ln\,(C/C_o)$ versus time (t) was obtained and the result is shown in Figure 8 (c). The plot was fitted with Langmuir-Hinshelwood pseudo first order equation with the rate constant of 0.0251 min^{-1}. Figure 8(d) represents the percentage reduction of Cr(VI) in the presence of MoS_2 nanosheets and shows that 91.05 % Cr(VI) reduction was achieved in 75 min.

3.2.4 Comparison of the effectiveness of the as-synthesized MoS_2 nanosheets with other published results

In order to ascertain the effectiveness of the as-synthesized MoS_2 nanosheets over other photocatalysts in the degradation of RhB and MB, and the reduction of Cr(VI), the photodegradation and photoreduction efficiencies of the MoS_2 nanosheets have been matched with other published data (Table 1). Taking into consideration the concentrations of the catalysts and the pollutants used, and the duration

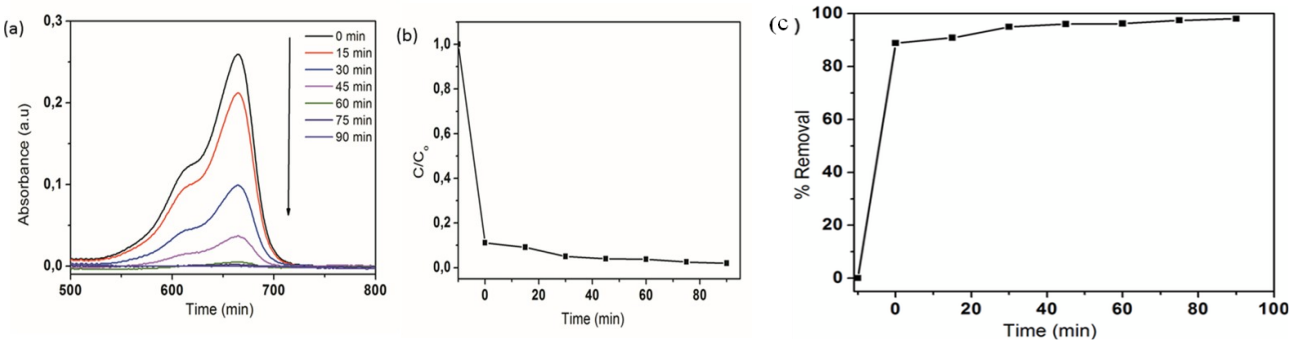

Figure 7. (a) UV–Vis spectroscopic changes of the MB aqueous solution in the presence MoS_2 nanosheets, (b) Photocatalytic degradation rate of MB as a function of time and (c) Percent removal of MB in the presence of MoS_2 nanosheets as a function of irradiation time

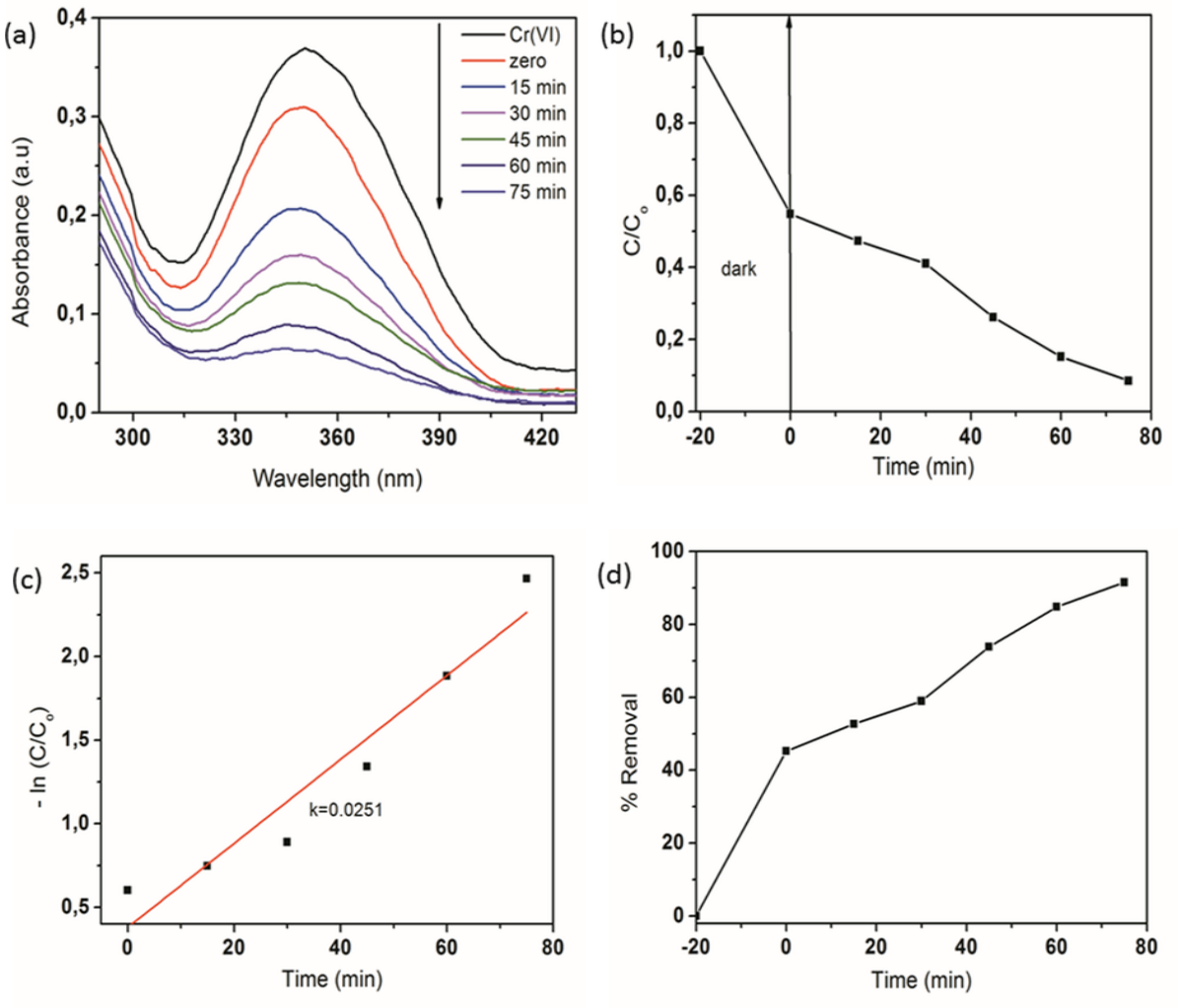

Figure 8. (a) UV-Vis absorption spectra of Cr(VI) reduction, (b) Photocatalytic reduction rate of Cr(VI), (c) Langmuir–Hinshelwood pseudo-first order kinetic plots or reduction of Cr(VI), and (d) Percent photoreduction of Cr(VI)

Table 1. Comparison of the effectiveness of the as-synthesized MoS_2 nanosheets with other published resultson the photodegradation of RhB and MB, and the photoreduction of Cr(VI) in wastewater using visible light

Catayst name	Pollutant name	Catalyst conc. (mg/L)	Pollutant conc. (mg/L)	Time (min)	Degradation (%)	Reference
CuS/PVA	RhB	20	50	60	80	[27]
Au/ZnO	RhB	100	20	60	87	[28]
$NaBiO_3$	RhB	100	20	180	97	[29]
PEG-MoS_2	RhB	50	10	90	97	[present work]
Pure MoS_2	RhB	50	10	90	72	[present work]
TiO_2	MB	20	20	300	86	[30]
ZnO-SnO_2	MB	400	20	60	96	[31]
TiO_2/AC	MB	20	50	90	98	[32]
PEG-MoS_2	MB	50	10	90	98	[present work]
Pure MoS_2	MB	50	10	90	76	[present work]
TiO_2	Cr(VI)	50	20	60	86	[33]
$NiFe_2O_4$-SiO_2	Cr(VI)	200	10	300	97	[34]
ZnO	Cr(VI)	1000	20	120	80	[35]
PEG-MoS_2	Cr(VI)	50	10	90	91	[present work]
Pure MoS_2	Cr(VI)	50	10	90	68	[present work]

of the photocatalytic experiments, the degradation efficiencies of the as-synthesized MoS_2 nanosheets evidenced that it is an effective catalyst as it showed much higher degradation efficiencies in the degradation of the two dyes and the reduction of Cr(VI) in comparison to the other photocatalysts used. In addition, the efficiency of the pure MoS_2 (MoS_2 without PEG 400) against the photodegradation of the two dyes (RhB and MB) and the photoreduction of Cr (VI) was also compared with that of the pegylated MoS_2 (Table 1). The results revealed that the pegylated MoS_2 displayed higher efficiencies in all the processes compared to the pure MoS_2. This observation indicates that the PEG 400, apart from acting as a capping agent, also enhanced the photodegradation efficiency of MoS_2.

3.2.5 Recyclability studies

The ability of the photocatalyst to be regenerated and re-used has been tested. This property is an important requirement as it will assist in reducing the cost associated with using new photocatalysts during each cycle. The outcome of this analysis (Figure 9) show only a small variation within the catalyst's reusability over the five cycles in the degradation of the dyes (RhB and MB) and the reduction of Cr(VI). The degradation efficiencies ranged from 97.3 % to 91.7 %, and 98.05 % to 92.2 % within the 80 min irradiation time for RhB and MB, respectively. Those of Cr(VI) reduction varied from 91.05 % to 89.25 %. The results indicate that the MoS_2 nanoparticle has the potential to be effectively recycled and re-used over a number cycles to proficiently degrade the dyes and reduce Cr(VI) to Cr(III) in aqueous medium.

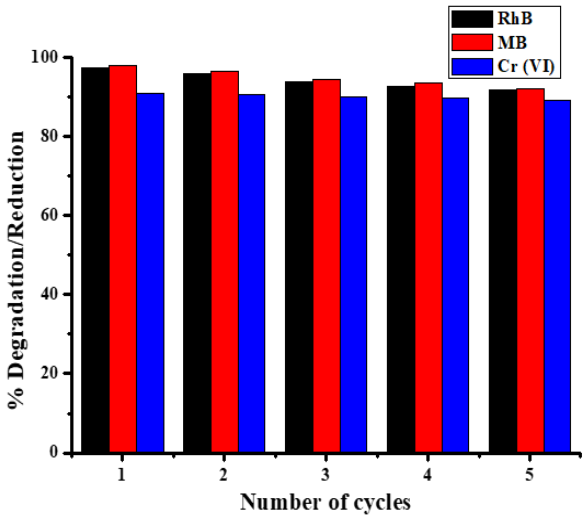

Figure 9. Recyclability study on MoS_2 nanosheets for the degradation of RhB, MB, and reduction of Cr(VI)

4. Conclusion

In summary, the microspheres of MoS_2 nanosheets were successfully synthesised by hydrothermal method. XRD reveals that the synthesised MoS_2 nanosheets can be indexed to hexagonal structure of MoS_2 (ICDD: 00-037-1492). SEM, TEM, and HRTEM images show that the synthesised sample has spherical shapes made up of several thin sheets of MoS_2 with the *d*-spacing of 0.682 nm. The energy band gap was estimated to be 1.92 eV. The RhB and MB dyes experienced degradation efficiencies of 97.30 % (RhB) and 98.05 % (MB) by the catalyst in 75 min 90 min, respectively in the presence of light. The results reveal that the synthesised MoS_2 nanosheet is a good photocatalytic material for degradation of dyes in water. It was also observed that light plays a crucial role in the degradation of the dyes. The catalyst is also observed to be effective in the photocatalytic reduction of Cr(VI). 91.05 % reduction of Cr(VI) to Cr(III) was achieved in 75 min.

Acknowledgements

The authors wish to express their gratitude to the Faculty of Science, University of Johannesburg and the DST/MSc Nanoscience Programme for their financial support toward this research.

References

[1] Hoffmann, M.R., Scot, T.M., Choi, W., Bahnemann, D.W. (1995). Environmental Applications of Semiconductor Photocatalysis. *Chemical Reviews*, 95: 69-96.

[2] Pouretedal, H.R., Norozi, A., Keshavarz, M.H., Semnani, A. (2009). Nanoparticles of Zinc Sulfide Doped with Manganese, Nickel and Copper as Nanophotocatalyst in the Degradation of Organic Dyes. *Journal of Hazardous Materials*, 162: 674-681.

[3] Sohrabnezhad, S.H. (2011). Study of Catalytic Reduction and Photodegradation of Methylene Blue by Heterogeneous Catalyst. *Spectrochimica Acta Part A: Molecular and Biomolecular Spectroscopy*, 81: 228-235.

[4] Martínez, S.S., Uribe, E.V. (2012). Enhanced Sonochemical Degradation of Azure B Dye by the Electrofenton Process. *Ultrasonics Sonochemistry*, 19: 174-178.

[5] Alluri, H.K., Ronda, S.R., Settalluri, V.S., Bondili, J.S., Suryanarayana, V., Venkateshwar, P. (2007). Biosorption: An Eco-Friendly Alternative for Heavy Metal Removal. *African Journal of Biotechnology*, 6: 2924-2931.

[6] Robinson, T., McMullan, G., Marchant, R., Nigam, P. (2001). Remediation of Dyes in Textile Effluent: A Critical Review on Current Treatment Technologies with a Proposed Alternative. *Bioresource Technology*, 77: 247-255.

[7] Slokar, Y.M., Le Marechal, A.M. (1998). Methods of Decoloration of Textile Wastewaters. *Dyes and Pigments*, 37: 335-356.

[8] Víctor-Ortega, M.D., Ochando-Pulido, J.M., Hodaifa, G., Martinez-Ferez, A. (2014). Final Purification of Synthetic Olive Oil Mill Wastewater Treated by Chemical Oxidation Using Ion Exchange: Study of Operating Parameters. *Chemical Engineering and Processing: Process Intensification*, 85: 241-247.

[9] Hu, H., Yang, M., Dang, J. (2005). Treatment of Strong Acid Dye Wastewater by Solvent Extraction. *Separation and Purification Technology*, 42: 129-136.

[10] Yagub, M.T., Sen, T.K., Afroze, S., Ang, H.M. (2014). Dye and Its Removal from Aqueous Solution by Adsorption: A Review. *Advances in Colloid and Interface Science*, 209: 172-184.

[11] Xu, L., Sun, Y., Du, L., Zhang, J. (2014). Removal of Tetracycline Hydrochloride from Wastewater by Nanofiltration Enhanced by Electro-Catalytic Oxidation. *Desalination*, 352: 58-65.

[12] Zhou, S., Watanabe, H., Wei, C., Wang, D., Zhou, J., Tatarazako, N., Masunaga, S., Zhang, Y. (2015). Reduction in Toxicity of Coking Wastewater to Aquatic Organisms by Vertical Tubular Biological Reactor. *Ecotoxicology and Environmental Safety*, 115: 217-222.

[13] Kudo, A., Miseki, Y. (2009). Heterogeneous Photocatalyst Materials for Water Splitting. *Chemical Society Reviews*, 38: 253-278.

[14] Chong, M.N., Jin, B., Chow, C.W., Saint, C. (2010). Recent Developments in Photocatalytic Water Treatment Technology: A Review. *Water Research*, 44: 2997-3027.

[15] Kramer, T.J., Babu, S.S., Saeki, A., Seki, S., Aimi, J., Nakanishi, T. (2012). CdSe Nanocrystal/C 60-Liquid Composite Material with Enhanced Photoelectrochemical Performance. *Journal of Materials Chemistry*, 22: 22370-22373.

[16] Sun, X.F., Liu, B., Jing, Z., Wang, H. (2015). Preparation and Adsorption Property of Xylan/Poly (Acrylic Acid) Magnetic Nanocomposite Hydrogel Adsorbent. *Carbohydrate Polymers*, 118: 16-23.

[17] Li, Y., Du, Q., Liu, T., Peng, X., Wang, J., Sun, J., Wang, Y., Wu, S., Wang, Z., Xia, Y., Xia, L. (2013). Comparative Study of Methylene Blue Dye Adsorption onto Activated Carbon, Graphene Oxide, and Carbon Nanotubes. *Chemical Engineering Research and Design*, 91: 361-368.

[18] Chitkara, M., Singh, K., Sandhu, I.S., Bhatti, H.S. (2011). Photo-Catalytic Activity of $Zn_{1-x}Mn_xS$ Nanocrystals Synthesised by Wet Chemical Technique. *Nanoscale Research Letters*, 6: 1-1

[19] Datta, A., Priyam, A., Bhattacharyya, S.N., Mukherjea, K.K., Saha, A. (2008). Temperature Tunability of Size in CdS Nanoparticles and Size Dependent Photocatalytic Degradation of Nitroaromatics. *Journal of Colloid and Interface Science*, 322: 128-135.

[20] Wu, C., Huang, X., Xie, L., Wu, X., Yu, J., Jiang, P. (2011). Morphology-Controllable Graphene–TiO_2 Nanorod Hybrid Nanostructures for Polymer Composites with High Dielectric Performance. *Journal of Materials Chemistry*, 21: 17729-17736.

[21] Chen, H., Nanayakkara, C.E., Grassian, V.H. (2012). Titanium Dioxide Photocatalysis in Atmospheric Chemistry. *Chemical Reviews*, 112: 5919-5948.

[22] Liu, G., Zhao, Y., Sun, C., Li, F., Lu, G.Q., Cheng, H.M. (2008). Synergistic Effects of B/N Doping on the Visible-Light Photocatalytic Activity of Mesoporous TiO_2. *Angewandte Chemie International Edition*, 47: 4516-4520.

[23] Asahi, R., Morikawa, T., Ohwaki, T., Aoki, K., Taga, Y. (2001). Visible-Light Photocatalysis in Nitrogen-Doped Titanium Oxides, *Science*, 293: 269-271.

[24] Macphee, D.E., Rosenberg, D., Skellern, M.G., Wells, R.P., Duffy, J.A., Killham, K.S. (2011). A Tungsten Oxide-Based Photoelectrocatalyst for Degradation of Environmental Contaminants, *Journal of Solid State Electrochemistry*, 15: 99-103.

[25] Lee, H.S., Min, S.W., Chang, Y.G., Park, M.K., Nam, T., Kim, H., Kim, J.H., Ryu, S., Im, S. (2012). MoS_2 Nanosheets Phototransistors with Thickness-Modulated Optical Energy Gap. *Nano Letters*, 12: 3695-3700.

[26] Wang, Q.H., Kalantar-Zadeh, K., Kis, A., Coleman, J.N., Strano, M.S. (2012). Electronics and Optoelectronics of Two-Dimensional Transition Metal Dichalcogenides. *Nature Nanotechnology*, 7: 699-712.

[27] Al-Kahtani, A.A. (2016). Photocatalytic Degradation of Rhodamine B Dye in Wastewater Using Gelatin/CuS/PVA Nanocomposites under Solar Light Irradiation. *Journal of Biomaterials and Nanobiotechnology*, 8: 66-68.

[28] Alshammari, A., Bagabas, A., Assulami, M (2014). Photodegradation of Rhodamine B over Semiconductor Supported Gold Nanoparticles: The Effect of Semiconductor Support Identity. *Arabian Journal of Chemistry*. doi.org/10.1016/j.arabjc.2014.11.013

[29] Yu, K., Yang, S., He, H., Sun, C., Gu, C., Ju, Y. (2009). Visible Light-Driven Photocatalytic Degradation of Rhodamine B over $NaBiO_3$: Pathways and Mechanism. *The Journal of Physical Chemistry A*, 113: 10024-10032.

[30] Dariani, R. S., Esmaeili, A., Mortezaali, A., Dehghanpour, S. (2016). Photocatalytic Reaction and Degradation of Methylene Blue on TiO_2 Nano-Sized Particles. *Optik-International Journal for Light and Electron Optics*, 127: 7143-7154.

[31] Lin, J., Luo, Z., Liu, J., Li, P. (2018). Photocatalytic Degradation of Methylene Blue in Aqueous Solution by Using ZnO-SnO_2 Nanocomposites. *Materials Science in Semiconductor Processing*, 87: 24-31.

[32] Ramli, C., Amali, Z., Asim, N., Isahak, W.N., Emdadi, Z., Ahmad-Ludin, N., Sopian, K. (2014). Photocatalytic Degradation of Methylene Blue under UV Light Irradiation on Prepared Carbonaceous. *The Scientific World Journal*, 2014: 1-8 (Article ID 415136, (doi:10.1155/2014/415136)

[33] Wu, Q., Zhao, J., Qin, G., Wang, C., Tong, X., Xue, S. (2013). Photocatalytic Reduction of Cr(VI) with TiO_2 Film under Visible Light. *Applied Catalysis B: Environmental*, 142: 142-148.

[34] Ojemaye, M.O., Okoh, O.O., Okoh, A.I. (2017). Performance of $NiFe_2O_4$-SiO_2-TiO_2 Magnetic Photocatalyst for the Effective Photocatalytic Reduction of Cr(VI) in Aqueous Solutions. *Journal of Nanomaterials*, 2017: 1-11 (Article ID 5264910, doi:10.1155/2017/5264910)

[35] Shirzad, S.M., Samadi, M.T., Yang, J.K., Lee, S.M. (2011). Photocatalytic Reduction of Cr (VI) and Ni (II) in Aqueous Solution by Synthesized Nanoparticle ZnO under Ultraviolet Light Irradiation: A Kinetic Study. *Environmental Technology*, 32: 1573-1579.